

Julia Cloud Matrix Machine: Dynamic Matrix Language Acceleration on Multicore Clusters in the Cloud

Jay Hwan Lee
jlee758@yonsei.ac.kr
Yonsei University
Seoul, South Korea

Yeonsoo Kim
yeonsoo.kim@yonsei.ac.kr
Yonsei University
Seoul, South Korea

Younghyun Ryu
usefulhyun@yonsei.ac.kr
Yonsei University
Seoul, South Korea

Wasuwee Sodsong
wasuwee.s@yonsei.ac.kr
Yonsei University
Seoul, South Korea

Hyunjun Jeon
wjsgus95@gmail.com
Yonsei University
Seoul, South Korea

Jinsik Park
pjshwa@gmail.com
Yonsei University
Seoul, South Korea

Bernd Burgstaller
bburg@yonsei.ac.kr
Yonsei University
Seoul, South Korea

Bernhard Scholz
Bernhard.Scholz@sydney.edu.au
University of Sydney
Sydney, Australia

Abstract

Matrix computations are widely used in increasing sizes and complexity in scientific computing and engineering. But current matrix language implementations lack programmer support to effectively and seamlessly utilize cloud computing resources. We extend the Julia high-performance compute language to automatically parallelize matrix computations for the cloud. Users are shielded from the complexity of explicitly-parallel computations through the provision of a novel matrix data type with lazy evaluation semantics. Delayed evaluation aggregates operations into expression trees that are rewritten on-the-fly to eliminate common subexpressions and apply optimizations such as exponentiation-by-squaring on matching subtrees. Trees are lowered into DAGs for which dynamic simulation selects the optimal tile size and execution schedule for a given cluster of cloud nodes. We employ off-line profiling to construct a time model for the compute and network capacity of the cluster. The experimental evaluation of our framework comprises eleven benchmarks on a cluster of eight nodes (288 vCPUs) in the AWS public cloud and reveals speedups of up to a factor of 4.11 \times , with an average 78.36 % of the theoretically possible maximum speedup.

CCS Concepts: • **Computing methodologies** \rightarrow *Shared memory algorithms; Parallel computing methodologies.*

Keywords: Matrix computations, Julia, HEFT, Distributed systems, Simulation, Parallel computing

1 Introduction

Matrix multiplication is a fundamental operation in scientific computing that has been intensively studied for parallel computing [1, 14, 39]. Utilizing a commodity cluster or the

cloud for matrix computations is complex due to the required concurrency control mechanisms. In terms of performance, the bottleneck is often the network rather than the memory bandwidth of a single node [10]. To maximize the performance of large computations, splitting them into smaller operations leverages parallelism, though at the cost of increased data communication. Striking a balance between the data communication bottleneck of the network and multicore parallelism is thus a key requirement to attain high performance in the cloud. Ideally, programmers are shielded from such considerations, if the underlying implementation of the sequential programming model can leverage the inherent parallelism for efficient execution in the cloud. This particularly applies to matrix languages like MATLAB, Octave and Julia, which are designed for programmer productivity and abstraction from the underlying multicore substrate, rather than hand-optimization of hardware-dependent code. To automatically parallelize matrix computations, our approach uses lazy evaluation in conjunction with hierarchical dependency analysis, online scheduling and simulation to effectively run tasks in parallel and reduce the impact of the network on performance. We implement this in Julia, a dynamic language for high performance computing that is already equipped with a robust, explicitly-parallel programming model [6]. The contributions of this paper are as follows:

- The Julia cloud matrix machine (Julia CMM) that extends the Julia programming language with implicitly-parallel matrix routines for the cloud through an extension of the Julia matrix data type.
- An online simulation and run-time that employs a time model based on offline profiling and regression analysis to predict task execution times. We utilize this in

conjunction with automatic matrix parallelization to predict the most efficient schedule of task parallelization across a cluster of cloud nodes.

- An extension of the HEFT scheduling algorithm that employs a node-level tile cache and a dynamic tiling optimization to reduce the network-incurred communication bottleneck.
- An extensive experimental evaluation on the AWS public cloud to show the validity of our approach.

2 Related Work

Level 1 BLAS covers vector-vector computations [22], level 2 BLAS covers vector-processing machines [12], and level 3 BLAS utilizes caches in a multi-memory hierarchy [11]. To take advantage of the cache, matrices are partitioned into smaller matrices to maximize the cache hit ratios [40, 41]. Julia uses OpenBLAS [30] as a multi-threaded level 3 BLAS implementation for linear algebra functions. Research into parallelization of BLAS operations for distributed systems exists [7, 31], yet they provide low-level BLAS operations, a static communication model, and static tile sizes. The proposed Julia CMM provides a high-level programming abstraction, a dynamic communication model, and dynamic tile sizes. Julia’s standard library provides the `RemoteChannel` and `SharedArray` primitives for intra- and inter-node communication, but programmers must manually parallelize their Julia code for the cloud.

There exists a large body of work in automatic parallelization of matrix-related operations, including optimizing compilers [3, 33], and the automated generation of an optimal parallel algorithm for matrix-vector multiplication in a neural network [28] (though the correctness of the latter is still indeterminate). Research in matrix multiplication optimizations for Intel processors [17, 29] is ongoing, but does not involve implicit parallelism like Julia CMM. Research into solving load imbalances has resulted in hybrid versions of the BFS and DFS algorithms for task-based parallelism [4], automatic tuning of sparse matrix-vector multiplications on multicore clusters equipped with a thread and process-based communication layer [23], automation of stream parallelism in C++ [25], and a selection prioritization modification of HEFT for cloud environments [16]. These frameworks, however, do not implement implicit parallelization for general matrix operations, and thereby are of more use to expert programmers than to the common user/domain expert.

Other implementations of the HEFT algorithm address issues with load imbalance in a cloud network, particularly where throughput is decreased due to creating idle resources from processing parent and child tasks with different input instances in parallel [44]. E-HEFT addresses this by reducing the number of communication tasks. The scheduler defines the task distribution across the nodes and a simulation is run [32]. We are already utilizing the node-level tile cache

to reduce the communication tasks and have already implemented a separate scheduler and simulation mentioned in the paper. Conversely, EHEFT-R utilizes remapping resource allocation rules to optimize optimal machines for the ranked tasks [43]. However, in a network where all machines are equal, ranking is not an effective optimization.

Scientific workflow research involves structuring a series of computations connected through dependencies [36] as a model for large-scale applications. In this structure, different tasks are scheduled to parallel resources with task scheduling optimization being construed as an NP-complete problem [38]. Wrt. a cloud environment, resource usage cost acts as an additional optimization point. Researchers proposed multi-objective scheduling algorithms [13, 26] as a solution in meeting multiple optimization constraints within a cloud environment, noting that multiple objectives inevitably result in trade-offs.

3 Julia CMM Framework

As depicted in Figure 1 step ①, Julia CMM is minimally invasive on the side of the user: the only adaptation required to parallelize sequential matrix code like the depicted Markov chain computation is to typecast matrices to the provided `ClusteredMatrix` data type (lines 2–3); The actual computations (lines 5–9) remain unchanged. Users write code in a Jupyter notebook [8] which is the frontend on the users’ laptop or desktop from where Julia CMM connects to the user’s rented cloud instances (the connection is established based on an MPI-like configuration file that lists the IP addresses of the cluster nodes and designates one node as the master).

Although users initiate execution of Julia CMM code on their client’s frontend, the actual computations take place in the cloud. Julia CMM employs lazy evaluation, which—at runtime—substitutes the execution of matrix operations with the construction of an expression tree, deferring the actual computation of operations until a result is required. E.g., for the Markov chain computation in Figure 1 step ①, the `for` loop iterates three times followed by the multiplication $u * M$, which will result in the expression tree depicted in Figure 1 step ②. Actual computation of the expression tree is triggered by the `display(M)` statement in line 11, which requires the result to be output to the user.

The advantage of lazy evaluation is to aggregate operations prior to their execution, thereby widening the optimization and parallelization *scope* from individual operations (the scope of, e.g., BLAS) to contiguous regions of operations in the execution trace. In our running example, the enlarged optimization scope enables the framework to detect the matrix exponentiation operation inherent in the expression tree (i.e., $P * P * P * P$), and rewrite it by employing exponentiation-by-squaring (step ③), to be further elaborated in Section 3.1). Eliminating the common subexpression $P * P$ results in the

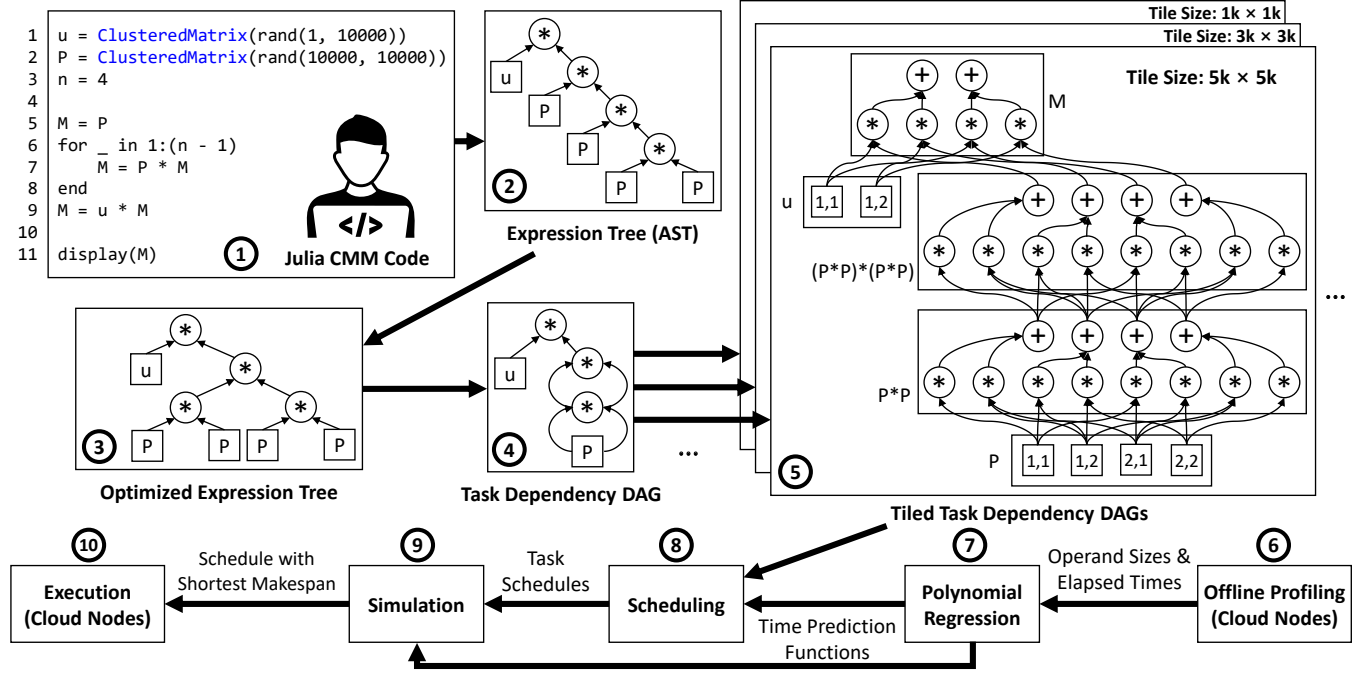


Figure 1. Overview of Julia CMM, depicting the on-the-fly lowering of the Markov chain benchmark source code ① to an expression tree ② that is then optimized by employing exponentiation by squaring ③. Common subexpression elimination creates a task dependency DAG ④ which is lowered further into tiled task dependency DAGs ⑤ for a series of standard tile sizes (here $1k \times 1k$, $3k \times 3k$, and $5k \times 5k$). Online scheduling ⑧ and simulation ⑨ of each of the tiled task dependency DAGs is used to determine the schedule with the smallest—predicted—makespan, which is then executed on the cluster of cloud nodes ⑩. The framework’s time model is based on offline profiling ⑥ and regression analysis ⑦.

task dependency DAG in step ④, which contains one matrix multiplication less than the original tree.

Likewise, lazy evaluation enlarges the parallelization scope, which enables Julia CMM to leverage a larger amount of parallelism and weigh its trade-off with the communication overhead that governs the tiling (i.e., splitting) of matrix operands into sub-operands (herein called tiles). Tiling reduces the granularity of work, which is necessary to utilize the parallel execution units of a cluster. However, smaller tiles increase the communication overhead. As depicted in Figure 1 step ⑤, Julia CMM lowers a task dependency DAG into a series of tiled dependency DAGs. Each tiled DAG encodes the *entire* task dependency DAG for one particular tile size. The purpose of creating tiled DAGs for a range of standard tile sizes is to conduct an online simulation that predicts the makespan of each tiled DAG and select the DAG with the shortest makespan for execution on the given cluster. Thereby the framework is able to weigh parallelism vs. communication overhead in the afore-mentioned trade-off.

Our online simulation employs a time model obtained from offline profiling (profile data is re-used if the framework is rerun on an already known instance type and location). Tiled DAGs under a modified HEFT algorithm are used to generate task schedules that optimize the earliest finish times.

Once the master node determines the schedule with the shortest makespan, it executes the schedule by using worker processes on the master and worker nodes. Workers send back their computed results to the master from where the results are output to the user on their client machine.

3.1 Tree-rewriting, Tiling, Scheduling & Simulation

Figure 1 uses a Markov chain computation to demonstrate the conversion from `ClusteredMatrix` in Julia CMM to tiled dependency graphs on the master node. References `P` and `u` point to `ClusteredMatrix` objects generated from random matrices according to the stated input dimensions. Matrix `P` is multiplied by `P` three times before the final multiplication by matrix `u`, as reflected in the expression tree in step ② of Figure 1. An expression tree constitutes a trace of matrix operations executed at runtime. Tree construction is facilitated by overloading the operators of the `ClusteredMatrix` data type. Edges in the expression tree constitute input dependencies, which are used to construct the task dependence graph. Lazy evaluation defers the actual execution of matrix operations until either a statement is reached that cannot be lazily evaluated because it constitutes a user-observable side-effect, or until the trace exceeds a pre-configured threshold. At that point, Julia CMM pattern-matches the constructed tree to

```

1 function tile(P::ClusteredMatrix, tile_size::Tuple)
2     mP, nP = size(P)
3     mTile, nTile = tile_size
4     mTiledP, nTiledP = cld(mP, mTile), cld(nP, nTile)
5     tiledP = Matrix{ClusteredMatrix}(mTiledP, nTiledP)
6
7     for j=1:nTiledP
8         colStart = nTile * (j-1)+1
9         colEnd = min(nTile * j, nP)
10        colIdx = colStart:colEnd
11        for i=1:mTiledP
12            rowStart = mTile * (i-1)+1
13            rowEnd = min(mTile * i, mP)
14            rowIdx = rowStart:rowEnd
15            tiledP[i,j] = view(P, rowIdx, colIdx)
16        end
17    end
18    return tiledP
19 end

```

Listing 1. Implementation of the tile function

re-write sub-trees for which a more efficient equivalent is known to exist. Thus, common subexpressions are eliminated [2], and series of multiplications are transformed into the exponentiation-by-squaring approach [20]. In comparison, standard Julia is not able to perform this optimization, unless the user manually replaces the for loop in Figure 1 with Julia’s exponentiation operator.

Tile sizes determine the granularity of partitioned matrix operations. Smaller tiles result in a larger number of suboperations and a higher level of parallelism. However, more suboperations imply increased internode communication overhead. In our experiments on the AWS cloud and our own commodity cluster, we observed that a tile size in the range of 10–50 % of the matrix size works best for most benchmarks, with not enough parallelism in tile sizes that exceed 50 %. When searching for an optimal tile size, we utilize time simulation with time models instead of using actual execution times. We thus generally use the sequence of tile sizes 1 k, 3 k, and 5 k for a matrix size of 10 k, with 5 k working best for most benchmarks of that matrix size. In Figure 1, the input matrix is of size 10 k, and the tile-size with the shortest predicted makespan is 5 k. The automatic tiling framework thereby generates four partitioned tiles of dimensions $5\text{ k} \times 5\text{ k}$ from matrix P , and two tiles of dimensions $1 \times 5\text{ k}$ from matrix u . The dependency graph changes accordingly with the tiles while preserving the task dependencies. Listing 1 shows the algorithm for tiling, which takes a matrix and tile size as arguments to return a tiled matrix, with tiles separated by tile dimensions (lines 8–15).

3.2 Dynamic Tiling Optimization

Once the master node commences the execution of the selected schedule, it is critical to propagate data and compute tasks instantly to worker nodes for computations to start on the worker nodes. Otherwise, CPU cores on the worker nodes will remain unutilized. We refer to the duration from the start of a schedule until every worker has received computation tasks as the *startup phase*. Figure 2a depicts the schedule of a master node (upper half) and one worker node

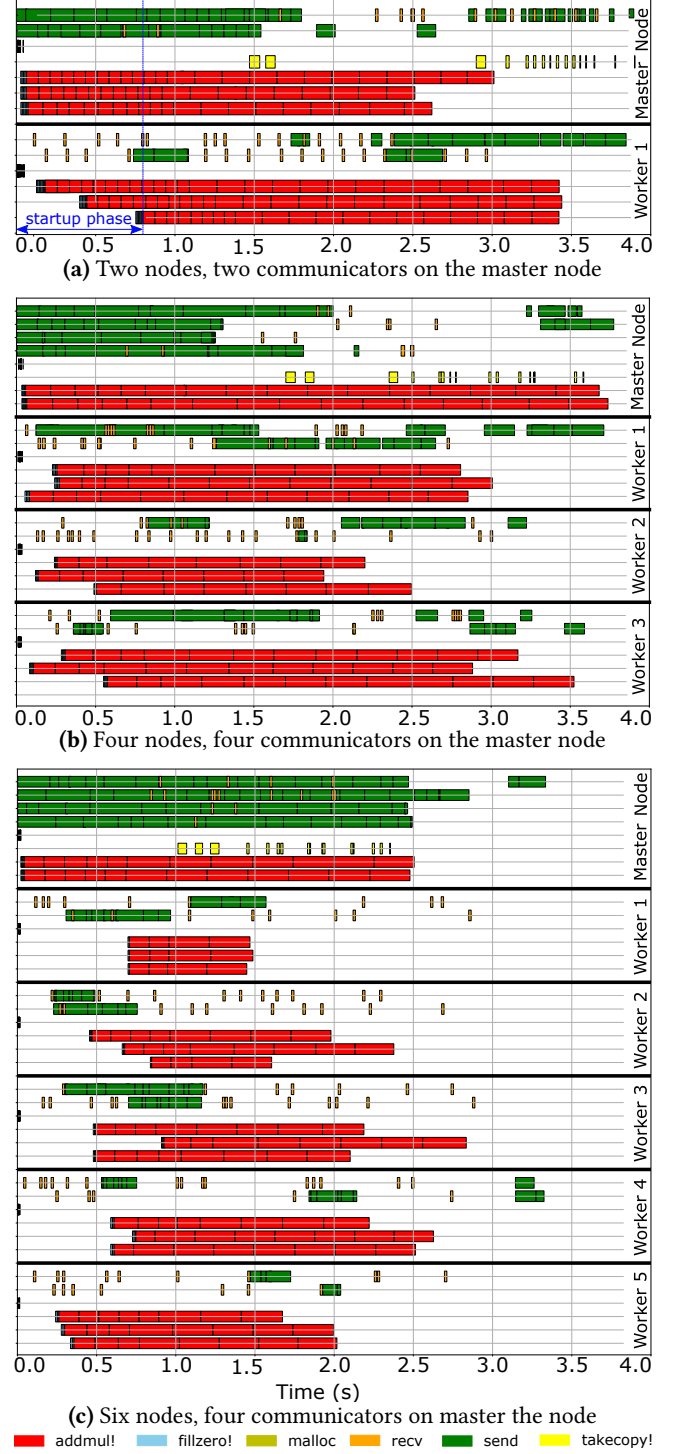


Figure 2. Markov chain benchmark task schedules for three cluster configurations of two, four, and six nodes on AWS c5.9xlarge instances using matrix sizes of 10 k and tile sizes of 3 k. Time flows from left to right. Schedules are visualized on a 4 s timeline to facilitate comparisons. Data send tasks (green) and matrix computations (red) dominate the schedules. The length of receive tasks (orange) is shorter than the corresponding send tasks.

Table 1. Interpolation based on the operand and operator sizes. The first two columns are the left and right operands, followed by the operators and the interpolation equation.

L Operand	R Operand	Operator	Interpolation Eqn.
$(n, 1)$	$(n, 1)$	$+, -, x$	$a_0 + a_1 n$
$(nm, 1)$	$(n, 1)$	x	$a_0 + a_1 n + a_2 m + a_3 mn$
(m, n)		\sin, \cos	$a_0 + a_1 n + a_2 m + a_3 mn$
(m, n)	1	$+, -, x, /$	$a_0 + a_1 n + a_2 m + a_3 mn$
(m, n)	(m, n)	$+, -, x$	$a_0 + a_1 n + a_2 m + a_3 mn$
(m, n)	(n, k)	x	$a_0 + a_1 n + a_2 m + a_3 k +$ $\dots + a_7 mnk$

(bottom half). Time moves from left to right. Green rectangles represent data send operations, and the two green bars at the top of Figure 2a signify that the two communication processes in the master node are continuously sending out data across the network to the worker node, denoted by “Worker 1”. Red rectangles represent compute tasks, and the blue arrow in the bottom-left of the figure indicates that it takes almost 0.75 s into the schedule until all three worker processes of Worker 1 have commenced computations (note that there are several matrix zeroing tasks denoted by blue rectangles at the beginning of the schedule, but they are of small duration and the constraining factor for the makespan is the time until data has arrived from the master node).

Given the network bandwidth cap that any given network imposes on simultaneous data transfers, we have observed that matrix tile sizes are large enough for the data send operations to a few worker nodes to monopolize the network and leave the remaining worker nodes starved: if the time to wait for previous communication tasks to finish plus the duration for sending data to a new worker node is predicted to take longer than waiting for a previous worker to become available, the scheduling algorithm inevitably favors scheduling on the latter. This results in both a large gap of time where workers are stalled waiting to receive data, and—in clusters with a larger number of nodes—workers that do not receive any data at all.

To mitigate this problem, we introduce dynamic tiling in the startup phase. When generating the tiled DAGs, tile sizes are dynamically adjusted such that large tiles are split into smaller sub-tiles to send more but smaller operands across the network in the same amount of time. This results in a non-homogeneous collection of tiles. Tile dependencies are preserved with smaller tiles being prioritized over larger tiles. During scheduling, sub-tiles are scheduled in the startup phase to bring work to all the workers in a smaller time. Once all workers in all nodes have work, further tiling into sub-tiles is unnecessary, and the schedule continues with the original tile sizes after all remaining sub-tiles have been scheduled. Sub-tiles are combined into tiles in-place after completion, allowing the different tile sizes to be seamlessly utilized in subsequent matrix operations.

As observed in Figure 2, worker nodes wait to receive data from the master node in the startup phase. Without dynamic tiling, the severity of the downtime is noticeably larger, and in larger networks, may result in some worker nodes never getting assigned a task. Dynamic tiling minimizes the startup phase by staging smaller tasks, and thus smaller communication costs *per task*, at the beginning of a schedule. As shown in Table 6, dynamic tiling achieves an overall speedup of $\geq 10\%$ for most benchmarks. We cover the results in-depth in Section 4.

3.3 Offline Profiling

Accurately predicting the execution time of each task is crucial to ensure the task allocation will minimize the total execution. We employ off-line profiling on a selection of typical matrix operations for the construction of the Julia CMM time model. Time measurements are based on CPU time-stamp counters (TSCs). For time duration measurements across nodes (where TSCs are typically unsynchronized), a novel technique that keeps the measurement error below 500 μ s is employed [42]. The off-line profiling step is conducted only once for a given cluster configuration.

The time model is constructed using multivariate polynomial regression analysis through the ordinary least square (OLS) method [21]. The amount of data is proportional to the size of the matrix, as is the number of floating point operations to the size of the operands. We thus make use of polynomial equations in predicting the execution time. Table 1 shows the classification for interpolation equations used in constructing the time predictions. The number of floating point operations to transmit is represented by a multivariate polynomial represented by the matrix size. The constants are obtained by regression analysis, and differ between each computation unit and node relationship.

3.4 Memory Management and Node-level Tile Cache

When a matrix operation is parallelized, it is partitioned into suboperations where an operand may be required by several successor operations. I.e., in the dependence DAG such an operand will have multiple successors (see, e.g., Fig. 1). Operands that are used multiple times will result in redundant communication if data is sent repeatedly to a given node. To mitigate such redundant inter-node communication, we introduced a node-level tile cache in a SharedArray in each node’s main memory. The SharedArray data type from the Julia standard library allows processes on the same node to share data. With this, data transferred from another node is maintained in the cache, to avoid re-sending of operands. Computation output on a node is directly designated to a tile allocated in the cache, to avoid memory copy operations between processes on the same node. Node-level tile caches are controlled by the scheduler: commands for the placement and eviction of operands in a node’s cache are already part

Table 2. Comparison of the simulation times of Julia CMM with and without the node-level tile cache for benchmarks in the Cell set, the Parboil set, and the Montage benchmark. The profiled data was obtained from two AWS c5.9x large instances (nodes) at a matrix size of 10 k.

Name	w/ cache	2 Nodes				8 Nodes			
		1 k	3 k	5 k	7 k	1 k	3 k	5 k	7 k
Markov	Y (s)	4.92	3.61	2.97	12.69	3.77	2.92	1.57	10.23
	N (s)	5.38	3.94	3.23	12.92	5.25	3.89	3.12	11.01
Kmeans	Y (s)	8.85	6.80	6.10	11.17	5.74	3.34	2.37	7.43
	N (s)	9.25	7.17	6.78	12.26	6.21	3.99	2.51	8.54
Hill	Y (s)	6.36	3.85	3.30	11.80	3.78	2.81	1.56	9.92
	N (s)	7.35	4.25	3.79	12.13	4.01	3.05	1.92	10.72
Leontief	Y (s)	9.70	8.78	7.98	15.81	6.58	5.05	4.01	11.77
	N (s)	10.56	9.82	8.80	16.62	6.89	5.49	4.43	12.60
Synth	Y (s)	6.47	4.83	4.82	12.69	3.97	3.09	1.40	11.60
	N (s)	7.23	5.28	5.62	13.86	5.14	4.16	3.34	12.28
Reach.	Y (s)	8.69	8.33	7.24	16.08	5.94	4.94	4.19	13.21
	N (s)	9.11	8.85	7.42	16.41	6.38	5.55	4.56	14.07
Hits	Y (s)	9.24	6.99	6.98	16.69	5.83	4.27	2.92	10.28
	N (s)	10.05	7.68	7.49	17.08	6.33	5.09	3.34	11.07
BFS	Y (s)	27.31	22.22	18.55	24.92	14.88	9.38	6.70	16.90
	N (s)	29.44	25.53	20.43	26.18	16.93	11.39	8.06	17.95
MM	Y (s)	36.91	31.93	23.47	33.00	13.90	13.50	10.77	21.93
	N (s)	39.04	34.91	26.53	35.31	16.45	15.90	12.90	23.07
SPMV	Y (s)	43.05	37.09	27.14	39.81	25.64	19.83	14.78	26.81
	N (s)	48.24	41.74	34.47	43.02	30.58	26.30	28.42	31.72
Montage	Y (s)	65.30	53.14	41.89	73.28	29.69	24.21	16.63	63.58
	N (s)	81.63	71.50	60.06	85.80	48.33	47.85	49.65	77.81

of the schedule, rather than guided by heuristics as it is done with caches in the CPU memory hierarchy. Likewise, the simulator anticipates the node-level tile caches in its predictions. As depicted in Table 2, there is a consistent performance improvement with the node-level tile cache implemented at varying tile and network sizes compared to without.

3.5 HEFT Scheduler Extension

We extend the heterogeneous earliest-finish-time (HEFT [37]) scheduling algorithm to make it aware of the node-level tile cache, such that it can effectively select optimal schedules. The original algorithm is split into two phases: a prioritizing phase where tasks are recursively ranked based on average

computation and communication costs across all nodes, and the second phase where tasks are assigned to processors such that the earliest finish time is selected. We utilize the average internode communication costs and adapt communication costs dynamically based on the presence of tiles in the node-level cache. The time predictions covered in Section 3.3 are utilized for obtaining the estimated times of each task. The scheduler takes communication time into account, which involves a send task from the sender and a receive task from the receiver (send times are asymmetrically longer than receive times due to sending data, as depicted in Figure 2). When recursively ranking the tasks, it prioritizes the smaller tile sizes. The accuracy of the generated schedules is proportional to the accuracy of the cost predictions.

There is always a small amount of latency in the startup phase of the schedule, where worker nodes must wait to receive data from the master. The scheduler prioritizes earliest finish time, and thus initially prefers worker processes on the master node due to it having no communication requirements. However, as the capacity of the master node is limited, worker nodes are utilized to minimize finish times. The scheduler rejects scheduling on a node if the combined communication and computation time is predicted to take longer than waiting for a node where the tile is already present to become available. Due to the master communicating with all workers, the master has more dedicated communication processes to process more communications tasks at once. In doing so, it reduces load imbalance that arises from stalling caused by communication tasks waiting to be scheduled.

4 Experimental Evaluation

For our evaluation of Julia CMM, we adopted benchmarks from a Cell Octave benchmark set [19], a set of highly parallelizable applications. We specifically took the Markov, K-Means, Hill, Leontief, Synth, Reachability, and Hits benchmarks and rewrote them in the Julia language. The Parboil Benchmark set [35] contains a set of throughput benchmarks for testing computer architecture in CUDA and OpenCL. We specifically adapted the BFS, MM, and SPMV benchmarks, which use matrix operations more predominantly than the others, and ported them to Julia. Pegasus [9] is a programming language for workflow applications such as CyberShake (earthquake testing) [15] and Sipht (searching untranslated RNAs) [24]. Pegasus utilizes DAGs in reproducing and analyzing scientific workflows, which share similarities with the schedules generated with our Julia framework. One application that uses Pegasus is the Montage Image Mosaic Engine [5], a tool for assembling astronomical input images into custom mosaics. We ported the Montage workflow written in Pegasus over to Julia that computes 3 separate color matrix channels to generate a small 2x2 image mosaic.

We used the Amazon EC2 service with instance type c5.9xlarge [34] as our environment. This instance type was

Table 3. GFLOPS performance of an AWS c5.9xlarge instance with Julia CMM, over 25 runs. The columns from left to right show the total number of threads, the number of communicators, workers (and threads per worker), average GFLOPS, and the coefficient of variation.

Total threads	Comm	Worker (threads)	GFLOPS Avg.	CoV (%)
4	1	3(1)	2,257.8	3.6
8	2	3(2)	1,186.3	5.9
12	3	3(3)	822.3	5.3
14	2	3(4)	720.9	7.3
16	4	3(4)	628.6	4.1
32	4	7(4)	629.1	6.5
64	8	7(8)	628.6	6.8

selected for having a guaranteed 10 Gbps network bandwidth in a shared network, and each instance provides 36 vCPUs (18 physical cores). Julia CMM was developed on version 1.0 of the Julia language.

In our experiments, we found that the ideal configuration for most benchmarks in Julia CMM uses two communication processes, three worker processes and four threads per worker. One worker process is comprised of the number of threads configured for BLAS, while one communication process contains one thread. Thus, in the ideal configuration, there are a total of 14 threads operating in a node. Table 3 shows the GFLOPS numbers for our framework based on the number of threads configured for an AWS c5.9xlarge instance. We find that resource oversubscription in a given node occurs at 16 threads or more. One c5.9xlarge instance has 36 vCPUs and 18 physical cores. Thus, adding more worker threads than the number of physical cores in a node causes thread competition utilizing resources, outweighing any potential benefit from introducing more worker processes.

Adding more communication processes tends to oversaturate the network bandwidth, which in turn worsens the latency of the individual send operations. Thus, with additional worker processes, the framework prefers utilizing the node-level tile cache in “seeded” nodes over sending matrix suboperations to new nodes.

Table 4 demonstrates the accuracy of the simulation is comparable with the execution of the benchmarks, with predicted values usually comprising a 5–20 % difference from actual values. The simulation thereby is at a point where its time model prediction is useful in effective task scheduling, particularly with the average simulation time being less than 0.2 s acting as a marginal overhead. There is overhead in managing the task dependencies during execution, causing the node-level tile cache to be slightly underestimated in the simulation, contributing to the slight accuracy deviation.

There is a common trend of performance improving with increasing tile sizes, as indicated in Table 5. With too small tile sizes, the communication overhead from more tasks is large enough to slow the benchmark down. However, the performance sharply degrades from 5 k to 7 k tile sizes for

Table 4. Julia CMM performance for tile sizes of 1 k, 3 k, and 5 k, at a matrix size of 10 k, averaged over 20 runs. “Exec. Time” depicts the execution times, “Pred. Time” depicts the execution time predicted by the simulation, “Acc.” depicts the accuracy of the prediction, and “Speedup” depicts the relative speedup from 1–8 nodes. The geometric mean speedups for all 11 benchmarks are listed at the end.

Name	Nodes	Exec. Time (s)			Pred. Time (s)			Acc. (%)			Speedup (1×)		
		1 k	3 k	5 k	1 k	3 k	5 k	1 k	3 k	5 k	1 k	3 k	5 k
Markov	1	10.78	8.57	6.52	10.20	7.71	6.04	106	111	108	1.00	1.00	1.00
	2	6.46	3.98	3.49	4.92	3.61	2.97	131	110	118	1.67	2.16	1.87
	4	4.94	3.75	3.04	4.14	2.81	2.86	119	134	106	2.18	2.28	2.15
	6	4.81	3.39	2.42	4.48	3.26	1.79	107	104	135	2.24	2.53	2.69
	8	3.85	3.00	1.78	3.77	2.92	1.57	102	103	113	2.80	2.86	3.66
Kmeans	1	14.56	12.07	8.87	12.86	10.08	7.55	113	120	117	1.00	1.00	1.00
	2	10.36	7.52	7.18	8.85	6.80	6.10	117	111	118	1.41	1.60	1.23
	4	7.65	6.79	6.20	6.72	5.44	5.12	114	125	121	1.90	1.78	1.43
	6	7.16	5.58	4.50	5.84	4.63	3.51	122	121	128	2.03	2.16	1.97
	8	6.44	3.92	2.59	5.74	3.34	2.37	112	117	109	2.26	3.08	3.43
Hill	1	12.79	9.43	6.80	10.17	7.90	6.12	126	119	111	1.00	1.00	1.00
	2	7.83	4.87	4.20	6.36	3.85	3.30	123	127	127	1.63	1.94	1.62
	4	7.10	4.56	3.71	5.35	3.74	2.80	133	122	132	1.80	2.07	1.83
	6	6.81	4.44	2.39	5.15	3.69	1.78	132	120	134	1.88	2.13	2.84
	8	4.57	2.93	1.79	3.78	2.81	1.56	121	104	115	2.80	3.22	3.79
Leontief	1	16.39	12.78	10.33	13.88	11.90	9.50	118	107	109	1.00	1.00	1.00
	2	12.36	10.86	10.09	9.70	8.78	7.98	127	124	126	1.33	1.18	1.02
	4	9.29	7.32	7.30	7.19	6.06	6.32	129	121	116	1.77	1.75	1.41
	6	8.92	6.97	6.02	7.07	6.45	4.96	126	108	121	1.84	1.83	1.72
	8	8.11	6.29	4.73	6.58	5.05	4.01	123	124	118	2.02	2.03	2.18
Synth	1	12.84	10.65	6.34	10.76	8.60	5.84	119	124	109	1.00	1.00	1.00
	2	8.14	5.59	5.54	6.47	4.83	4.82	126	116	115	1.58	1.91	1.14
	4	8.15	5.17	5.27	6.36	4.60	4.58	128	112	115	1.58	2.06	1.20
	6	5.68	3.81	2.44	4.33	3.02	2.22	131	126	110	2.26	2.79	2.60
	8	4.36	3.63	1.54	3.97	3.09	1.40	110	118	110	2.95	2.93	4.12
Reachability	1	13.39	11.30	10.75	11.04	11.00	9.02	121	103	119	1.00	1.00	1.00
	2	11.16	9.87	9.28	8.69	8.33	7.24	128	118	128	1.20	1.14	1.16
	4	8.95	8.95	9.08	7.78	6.99	7.25	115	128	125	1.50	1.26	1.18
	6	9.10	8.15	7.76	7.24	6.80	6.83	126	120	114	1.47	1.39	1.38
	8	7.79	5.43	5.03	5.94	4.94	4.19	131	110	120	1.72	2.08	2.14
Hits	1	16.23	13.29	10.87	14.85	11.70	9.72	109	114	112	1.00	1.00	1.00
	2	11.01	8.34	8.83	9.24	6.99	6.98	119	119	127	1.48	1.59	1.23
	4	10.60	7.88	7.01	8.51	7.18	5.94	124	110	118	1.53	1.69	1.55
	6	9.15	7.53	6.20	7.04	5.96	5.34	130	126	116	1.77	1.77	1.75
	8	7.03	4.90	3.70	5.83	4.27	2.92	120	115	127	2.31	2.71	2.94
BFS	1	35.76	27.90	22.43	33.30	23.02	21.48	107	121	104	1.00	1.00	1.00
	2	29.81	22.08	21.00	27.31	20.22	18.55	109	109	113	1.20	1.26	1.07
	4	22.51	19.49	16.06	21.10	18.17	14.09	107	107	114	1.59	1.43	1.40
	6	19.61	17.35	13.42	18.08	15.45	12.59	108	112	107	1.82	1.61	1.67
	8	15.96	10.47	8.35	14.88	9.38	6.70	107	112	125	2.24	2.66	2.69
MM	1	48.52	42.63	34.40	41.13	35.11	31.92	118	121	108	1.00	1.00	1.00
	2	43.29	33.11	31.51	36.91	31.93	23.47	117	104	134	1.12	1.29	1.09
	4	34.25	29.08	22.28	28.19	25.16	19.72	122	116	113	1.42	1.47	1.54
	6	18.23	24.05	17.85	17.29	22.06	17.30	105	109	103	2.66	1.77	1.93
	8	15.47	14.80	11.70	13.90	13.50	10.77	111	110	109	3.14	2.88	2.94
SPMV	1	57.30	51.63	41.90	52.10	47.02	40.82	110	110	103	1.00	1.00	1.00
	2	47.18	41.68	33.30	43.05	37.09	27.14	110	112	123	1.21	1.24	1.26
	4	42.67	31.44	30.70	40.59	29.27	25.85	105	107	119	1.34	1.64	1.36
	6	34.66	24.20	25.06	31.75	21.36	22.02	109	113	114	1.65	2.13	1.67
	8	28.11	20.72	18.27	25.64	19.83	14.78	110	104	124	2.04	2.49	2.29
Montage	1	89.59	82.97	67.18	81.31	75.44	66.52	110	110	101	1.00	1.00	1.00
	2	72.00	61.84	49.11	65.30	53.14	41.89	110	116	117	1.24	1.34	1.37
	4	60.58	53.45	43.41	55.39	48.05	37.89	109	111	115	1.48	1.55	1.55
	6	49.31	39.92	28.39	44.62	32.60	22.20	111	122	128	1.82	2.08	2.37
	8	35.89	29.78	20.34	29.69	24.21	16.63	121	123	122	2.50	2.79	3.30
Geomean 11 benchm.	1	–	–	–	–	–	–	–	–	–	1.00	1.00	1.00
	2	–	–	–	–	–	–	–	–	–	1.36	1.49	1.25
	4	–	–	–	–	–	–	–	–	–	1.63	1.70	1.48
	6	–	–	–	–	–	–	–	–	–	1.93	1.98	2.01
	8	–	–	–	–	–	–	–	–	–	2.40	2.68	2.96

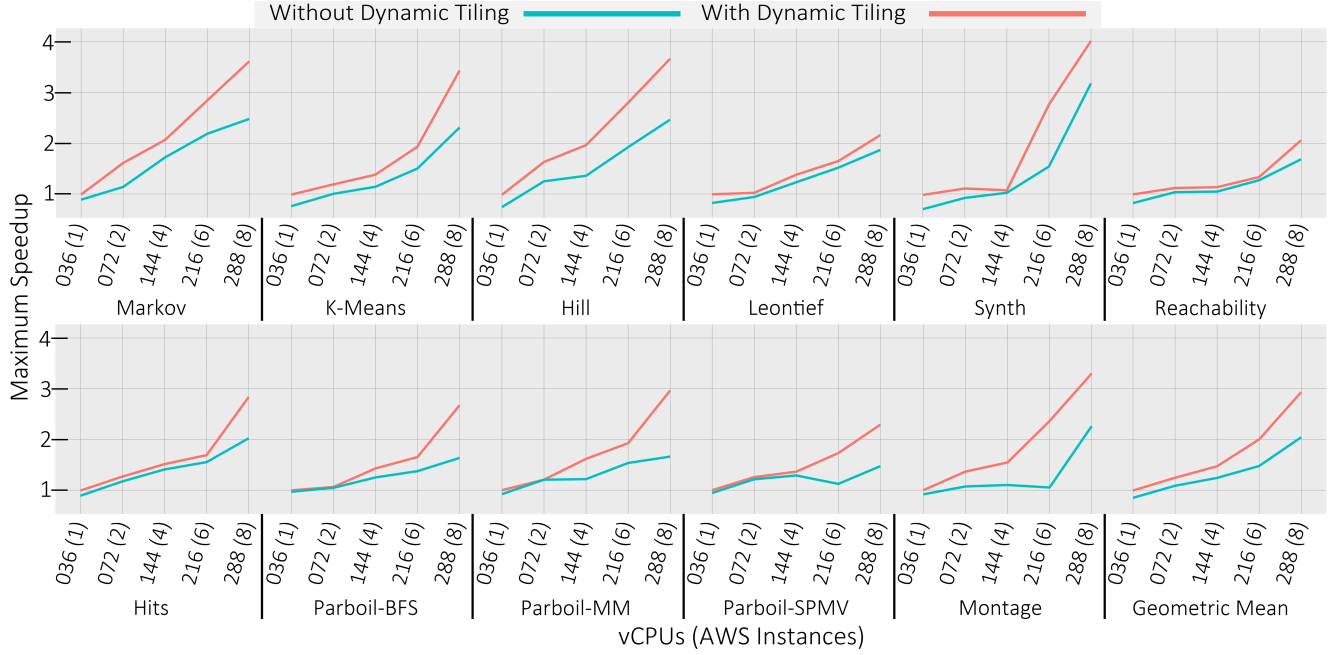


Figure 3. Julia CMM speedups with and without dynamic tiling over vanilla Julia on c5.9xlarge AWS instances from one node (36 vCPUs) to eight nodes (288 vCPUs in total). Julia CMM (the entire computation, including online simulation) is compared against the time to execute the benchmark in vanilla Julia on a single node. All benchmarks were run with a matrix size of 10 k, with the simulated tile sizes ranging from 1 k to 5 k. The tile size that resulted in the highest performance in the online simulation is automatically selected by the framework, and presented here. The last diagram depicts the geometric mean across all benchmarks.

all benchmarks. If the tile sizes are too large, not enough parallelism takes place in the framework. Since most benchmarks see their best performance in the 5 k tile size range, all benchmark results are presented with a tile size of 5 k as the default. Only simulation times are used in this comparison, as we have shown that the accuracy of simulation is comparable with execution in Table 4.

Figure 2 on page 4 demonstrates the results of scheduling tasks for the Markov benchmark with an increasing number of nodes in the network. The memory allocation tasks `malloc` are scheduled first on each node followed by data initialization tasks `fillzero`. Communication tasks are separated into `send`, a request to send data to another node, and `recv`, an indication that the node received data. Matrix addition and multiplication take place in computation tasks `addmul!`. Finally, `takecopy!` copies data from worker nodes into the master for the final matrix computation.

Figure 2a depicts a network with just the master and one worker node, and the schedule contains a total of 421 CMM tasks. Communication is sparse with the low number of nodes, being dominant at the beginning (sending data to the worker node) and at the end (receiving data from the worker node). Thus, only two communication processes in the master is sufficient to ensure good load balance. With more nodes, as depicted in Figure 2b, two communication processes in the master is insufficient to ensure a balanced

workload across the network. Processes would be busy when waiting to schedule new communication requests, and there is a higher number of tasks to schedule, with 579 CMM tasks in the depicted schedule. More communication processes in the master thereby improves load balance by allowing communication requests to be finished earlier. However, it is naive to add an arbitrary number of communicators, as too many causes network contention by saturating the network with excess requests.

A feature common with all schedules is that the first workloads on worker nodes are scheduled after the first workloads on the master node. No communication is needed to schedule tasks on the master node, whereas worker nodes wait to receive data from the master node. It reflects on the communication bottleneck where the duration of the startup phase is made more prominent with more nodes in the network.

Table 6 demonstrates the performance improvement from implementing the dynamic tiling optimization. For ≥ 2 nodes in most benchmarks, it results in a $\geq 10\%$ speedup. The improvement is most apparent with Montage at 276%, which is due to it already being structured as a workflow that is flexible to dynamic tile sizes. We observe a general trend that with increasing input matrix size, the performance improvement with the optimization gradually decreases. This can be attributed to the tile size of 5 k comprising a smaller portion of a larger matrix, and thus not affecting the overall

Table 5. Simulation time comparison of tile sizes from 1 k to 9 k in 1 k increments, at a matrix size of 10 k (averages over 20 runs per tile size stated). It is based on the benchmarks from the Cell set, the Parboil set, and the Montage benchmark.

Name	Nodes	Simulation Time (s)								
		1 k	2 k	3 k	4 k	5 k	6 k	7 k	8 k	9 k
Markov	1	10.20	8.86	7.71	6.95	6.04	8.14	20.76	21.60	22.95
	2	4.92	4.60	3.61	3.22	2.97	6.46	12.69	13.92	17.09
	4	4.14	3.94	2.81	2.42	2.86	3.21	11.35	13.48	16.39
	6	4.48	3.48	2.42	2.19	1.79	1.84	10.14	12.32	13.19
	8	3.77	3.10	2.92	2.39	1.57	1.23	10.23	11.98	14.42
Kmeans	1	12.86	10.25	10.08	8.15	7.55	8.63	18.43	20.00	21.66
	2	8.85	7.46	6.80	6.33	6.10	7.73	11.17	13.72	16.04
	4	6.72	5.82	5.44	5.05	5.12	6.99	9.58	11.04	13.41
	6	5.84	4.60	4.63	4.05	3.51	4.59	7.68	10.21	12.07
	8	5.74	4.62	3.34	2.73	2.37	4.90	7.43	8.63	9.61
Hill	1	10.17	8.95	7.90	6.36	6.12	8.82	17.86	19.33	21.34
	2	6.36	5.08	3.85	3.66	3.30	7.99	11.80	12.88	13.87
	4	5.35	4.55	3.74	3.54	2.80	4.49	9.42	10.23	12.67
	6	5.15	4.79	3.69	2.77	1.78	4.60	9.39	10.25	12.41
	8	3.78	3.66	2.81	1.61	1.56	4.70	9.92	10.71	12.71
Leontief	1	13.88	13.09	11.90	9.43	9.50	11.70	21.83	24.30	26.60
	2	9.70	9.39	8.78	8.01	7.98	10.45	15.81	16.96	19.06
	4	7.19	6.72	6.06	5.75	6.32	10.56	13.86	16.00	18.78
	6	7.07	6.89	6.45	5.47	4.96	9.37	12.56	12.86	13.60
	8	6.58	5.77	5.05	4.23	4.01	9.74	11.77	12.28	14.94
Synth	1	10.76	9.28	8.60	6.32	5.84	8.70	16.83	18.13	19.87
	2	6.47	5.43	4.83	4.64	4.82	7.98	12.69	14.39	16.72
	4	6.36	5.56	4.60	4.30	4.58	8.44	11.82	14.45	15.47
	6	4.33	3.53	3.02	2.06	2.22	7.52	10.44	12.85	14.65
	8	3.97	3.17	3.09	1.67	1.40	8.58	11.60	13.03	14.74
Reachability	1	11.04	11.34	11.00	10.50	9.02	10.43	21.02	22.07	23.48
	2	8.69	8.54	8.33	7.67	7.24	9.22	16.08	16.80	18.46
	4	7.78	6.82	6.89	6.02	7.25	9.52	14.60	15.13	17.37
	6	7.24	6.19	6.00	5.60	6.83	8.21	13.99	14.92	17.98
	8	5.94	5.67	4.94	3.92	4.19	8.74	13.21	15.12	17.43
Hits	1	14.85	13.32	11.70	10.37	9.72	13.73	21.49	22.71	24.89
	2	9.24	8.57	6.99	6.86	6.98	11.86	16.69	19.13	21.65
	4	8.51	7.32	7.18	6.21	5.94	12.34	14.92	16.62	18.42
	6	7.04	6.59	5.96	4.90	5.34	11.38	13.90	15.41	15.80
	8	5.83	5.32	4.27	3.01	2.92	10.09	10.28	11.13	12.73
BFS	1	33.30	29.15	23.02	22.54	21.48	25.67	30.38	34.45	37.28
	2	27.31	23.73	22.22	20.02	18.55	20.50	24.92	30.23	37.53
	4	21.10	19.99	18.17	16.25	14.09	19.88	24.15	24.35	29.26
	6	18.08	16.03	15.45	13.84	12.59	15.64	21.37	23.01	24.40
	8	14.88	12.66	9.38	7.34	6.70	11.32	16.90	18.69	22.04
MM	1	41.13	38.32	35.11	33.72	31.92	35.59	36.69	44.77	46.57
	2	36.91	34.36	31.93	28.13	23.47	30.43	33.00	37.47	45.33
	4	28.19	27.73	25.16	22.31	19.72	27.58	35.24	37.52	37.51
	6	17.29	20.46	22.06	20.13	17.30	23.12	28.95	27.60	31.09
	8	13.90	13.87	13.50	11.52	10.77	18.69	21.93	23.57	28.71
SPMV	1	52.10	49.14	47.02	42.15	40.82	40.58	47.94	49.17	55.01
	2	43.05	41.94	37.09	34.75	27.14	31.59	39.81	42.58	52.81
	4	40.59	31.85	29.27	27.24	25.85	35.70	37.80	40.34	44.19
	6	31.75	26.60	21.36	21.86	22.02	35.50	34.86	36.69	45.24
	8	25.64	23.34	19.83	16.42	14.78	21.34	26.81	33.70	39.73
Montage	1	81.31	78.38	75.44	70.05	66.52	78.31	80.60	88.37	95.35
	2	65.30	61.66	53.14	49.44	41.89	61.01	73.28	75.77	80.29
	4	55.39	52.91	48.05	42.45	37.89	68.35	70.98	70.35	73.36
	6	44.62	38.17	32.60	29.70	22.20	54.33	63.16	71.94	77.37
	8	29.69	25.24	24.21	21.79	16.63	56.47	63.58	65.29	73.94

Table 6. Comparison of the performance achieved with the dynamic tiling optimization. It further makes comparisons between matrix sizes of 10 k, 15 k, and 20 k, at a tile size of 5 k. The columns depict the original simulation time, the improved time with dynamic tiling, and the relative speedup compared to without the optimization. The geometric mean of the speedups for all 11 benchmarks are listed at the end.

Name	Nodes	Original (s)			Optimized (s)			Speedup (1×)		
		10 k	15 k	20 k	10 k	15 k	20 k	10 k	15 k	20 k
Markov	1	6.15	11.99	17.38	6.04	11.91	16.81	1.02	1.01	1.03
	2	4.80	10.49	15.97	2.97	9.10	14.46	1.61	1.15	1.10
	4	4.17	8.74	14.54	2.86	7.79	13.09	1.46	1.12	1.11
	6	3.00	7.63	14.24	1.79	6.43	12.64	1.67	1.19	1.13
	8	2.60	7.83	13.34	1.57	6.45	11.66	1.66	1.21	1.14
Kmeans	1	7.64	13.62	18.23	7.55	13.18	18.23	1.01	1.03	1.00
	2	6.78	10.92	16.92	6.10	9.49	15.06	1.11	1.15	1.12
	4	5.58	10.09	16.27	5.12	9.17	14.04	1.09	1.10	1.16
	6	3.86	9.74	15.64	3.51	8.42	13.78	1.10	1.16	1.14
	8	2.51	7.70	13.81	2.37	6.80	11.63	1.06	1.13	1.19
Hill	1	6.39	12.25	17.59	6.12	11.85	17.43	1.04	1.03	1.01
	2	3.79	8.98	15.02	3.30	8.10	13.80	1.15	1.11	1.09
	4	3.28	8.98	14.81	2.80	7.92	13.42	1.17	1.13	1.10
	6	2.06	7.66	13.99	1.78	6.63	12.02	1.16	1.15	1.16
	8	1.92	7.82	13.23	1.56	6.69	11.73	1.23	1.17	1.13
Leontief	11	10.06	15.58	21.22	9.50	15.09	20.63	1.06	1.03	1.03
	2	8.80	14.23	20.04	7.98	12.14	18.49	1.10	1.17	1.08
	4	6.73	12.27	18.35	6.32	10.31	15.37	1.06	1.19	1.19
	6	5.45	11.24	16.74	4.96	9.58	14.61	1.10	1.17	1.15
	8	4.43	9.50	16.43	4.01	7.90	14.71	1.11	1.20	1.12
Synth	1	6.08	11.92	17.58	5.84	11.76	17.26	1.04	1.01	1.02
	2	5.62	9.71	16.09	4.82	8.33	14.86	1.17	1.17	1.08
	4	6.16	10.07	15.17	4.58	9.03	13.52	1.34	1.12	1.12
	6	4.76	7.98	14.08	2.22	6.88	12.52	2.15	1.16	1.12
	8	3.34	6.56	12.57	1.40	5.49	11.08	2.38	1.19	1.13
Reachability	1	9.36	15.33	20.66	9.02	14.82	19.96	1.04	1.03	1.03
	2	7.42	13.17	19.00	7.24	11.57	17.22	1.02	1.14	1.10
	4	7.65	12.98	18.50	7.25	11.48	17.13	1.05	1.13	1.08
	6	7.05	11.68	17.09	6.83	10.72	15.00	1.03	1.09	1.14
	8	4.56	9.95	15.85	4.19	8.43	13.24	1.09	1.18	1.20
Hits	1	9.87	15.09	21.16	9.72	14.76	20.83	1.02	1.02	1.02
	2	7.49	12.93	19.09	6.98	11.44	17.60	1.07	1.13	1.08
	4	6.24	11.72	17.62	5.94	10.13	16.27	1.05	1.16	1.08
	6	5.67	10.84	16.92	5.34	9.02	14.98	1.06	1.20	1.13
	8	3.34	9.75	15.74	2.92	7.93	13.61	1.15	1.23	1.16
BFS	1	22.06	31.79	48.52	21.48	30.92	47.3	1.03	1.03	1.03
	2	20.43	27.19	45.07	18.55	23.49	35.44	1.10	1.16	1.27
	4	17.08	22.69	39.69	14.09	18.96	28.14	1.21	1.20	1.41
	6	15.54	19.15	37.41	12.59	16.97	21.84	1.23	1.13	1.71
	8	8.06	17.29	36.87	6.70	12.59	17.74	1.20	1.37	2.08
MM	1	33.12	47.51	71.62	31.92	46.56	69.82	1.04	1.02	1.03
	2	26.53	35.26	62.97	23.47	32.05	52.92	1.13	1.10	1.19
	4	23.24	34.84	59.38	19.72	22.17	40.06	1.18	1.57	1.48
	6	19.40	29.92	55.91	17.30	15.98	27.34	1.12	1.87	2.04
	8	12.90	28.93	47.05	10.77	12.64	19.27	1.20	2.29	2.44
SPMV	1	41.70	49.48	73.15	40.82	48.06	72.08	1.02	1.03	1.01
	2	34.47	40.35	68.36	27.14	37.12	51.23	1.27	1.09	1.33
	4	32.49	38.89	62.46	25.85	30.6	45.11	1.26	1.27	1.38
	6	37.29	39.24	55.33	22.02	24.66	38.89	1.69	1.59	1.42
	8	28.42	34.68	49.88	14.78	19.19	27.23	1.92	1.81	1.83
Montage	1	68.24	80.94	106.43	66.52	78.41	104.87	1.03	1.03	1.01
	2	60.06	77.13	97.66	41.89	60.81	76.22	1.43	1.27	1.28
	4	58.00	76.11	93.33	37.89	47.13	61.24	1.53	1.61	1.52
	6	61.76	73.1	89.38	22.20	32.29	47.89	2.78	2.26	1.87
	8	49.65	69.29	85.66	16.63	18.45	33.52	2.98	3.76	2.56
Geomean 1 benchm.	1	-	-	-	-	-	-	1.03	1.02	1.02
	2	-	-	-	-	-	-	1.33	1.15	1.16
	4	-	-	-	-	-	-	1.35	1.23	1.23
	6	-	-	-	-	-	-	1.62	1.32	1.33
	8	-	-	-	-	-	-	1.87	1.47	1.46

Table 7. The speedups are based on a configuration using eight nodes, a matrix size of 10 k, and a tile size of 5 k. Observed speedups are calculated by comparing the time obtained with eight nodes to that with one node, as seen in Table 4, without the dynamic tiling optimization. New speedups are then calculated with the dynamic tiling optimization implemented. Theoretical speedups assume zero communication time.

Benchmark Name	Observed Speedup (1×)	Dynamic Tiling (1×)	Theoretical Speedup (1×)
Markov	2.92	3.65	4.02
Kmeans	2.48	3.48	3.88
Hill	3.02	3.71	4.39
Leontief	2.14	2.18	3.90
Synth	3.49	4.11	4.23
Reachability	1.74	2.08	3.96
Hits	1.91	2.86	3.95
BFS	2.15	2.68	3.40
MM	2.21	2.97	3.75
SPMV	1.48	2.29	3.07
Montage	2.02	3.30	3.82

schedule as much. A large starting tile size in a larger matrix size of 20 k results in longer individual tasks to schedule, which does not scale well with the optimization.

Figure 3 depicts the maximum speedups of eleven benchmarks from one node (36 vCPUs) to eight nodes (288 vCPUs). We use the geometric mean [18, 27] to represent the maximum speedup across all benchmarks. Most maximum speedups exceed 2×, with some reaching 3×. The Markov benchmark reaches a speedup of 3.62× with the best performing tile size, and the Synth benchmark reaches 4.02× maximum speedup compared to vanilla Julia. We find the parallelization performance improves with more nodes in the network. For all configurations, the dynamic tiling optimization results in a better performance, particularly when there are more nodes in the network, as it helps to mitigate the communication bottleneck in such cases. Dynamic tiling ensures that all workers are active, and the node-level tile cache ensures they remain active, resulting in a higher performance with more nodes. Synth appears extreme as it uses many small independent matrix operations that introduce a relatively higher number of communication tasks which slow the network down, where introducing more nodes helps to spread the workload around.

We calculate the theoretical maximum speedup for each benchmark by setting the communication speed and latency to zero in the simulation, meaning that communication is instantaneous. All the tasks are already parallelizable and asynchronous, so communication acts as the bottleneck to achieving full parallelism in a distributed system. The other parameters remain the same: eight nodes with a matrix size of 10 k and tile size of 5 k. As Table 7 shows, with dynamic tiling, most benchmarks do not significantly deviate from the theoretical speedups, being in the range of 10–52 % from

the maximum speedup. It is not feasible to achieve the theoretical speedup in reality due to necessitating instantaneous communication, so some deviation is expected.

5 Conclusions

We proposed the CMM framework which extends the Julia language to automatically parallelize matrix computations for the cloud with minimal user intervention. The framework employs offline profiling to generate accurate time prediction models using polynomial regression. They are used with tiled dependencies by the modified HEFT scheduler to allocate tasks such that overall execution time is minimized. Communication overhead optimizations are made by introducing additional communication processes, dynamic tiling, and the node-level tile cache. We conducted an extensive experimental evaluation on a set of benchmarks using up to eight nodes (288 vCPUs) in the AWS public cloud. Our framework achieved speedups of up to a factor of 4.11×, with an average 78.36 % of the theoretical maximum speedup.

References

- [1] R. C. Agarwal, F. G. Gustavson, and M. Zubair. 1994. A high-performance matrix-multiplication algorithm on a distributed-memory parallel computer, using overlapped communication. *IBM Journal of Research and Development* 38, 6 (1994), 673–681. <https://doi.org/10.1147/rd.386.0673>
- [2] Alfred V. Aho, Monica S. Lam, Ravi Sethi, and Jeffrey D. Ullman. 2006. *Compilers: Principles, Techniques, and Tools* (2nd ed.). Addison-Wesley Longman Publishing Co., Inc., USA.
- [3] Serguei Diaz Baskakov and Juan Gutierrez Cardenas. 2021. Source to source compiler for the automatic parallelization of JavaScript code. In *2021 IEEE XXVIII International Conference on Electronics, Electrical Engineering and Computing (INTERCON)*. IEEE, 1–4.
- [4] Austin R. Benson and Grey Ballard. 2015. A Framework for Practical Parallel Fast Matrix Multiplication. In *Proceedings of the 20th ACM SIGPLAN Symposium on Principles and Practice of Parallel Programming (San Francisco, CA, USA) (PPoPP 2015)*. Association for Computing Machinery, New York, NY, USA, 42–53. <https://doi.org/10.1145/2688500.2688513>
- [5] G. Bruce Berriman and J. C. Good. 2017. The Application of the Montage Image Mosaic Engine to the Visualization of Astronomical Images. *Publications of the Astronomical Society of the Pacific* 129, 975 (2017), 1–15. <https://www.jstor.org/stable/26660114>
- [6] Jeff Bezanson, Alan Edelman, Stefan Karpinski, and Viral B Shah. 2017. Julia: A fresh approach to numerical computing. *SIAM review* 59, 1 (2017), 65–98. <https://doi.org/10.1137/141000671>
- [7] L Susan Blackford, Jaeyoung Choi, Andy Cleary, Eduardo D’Azevedo, James Demmel, Inderjit Dhillon, Jack Dongarra, Sven Hammarling, Greg Henry, Antoine Petitet, et al. 1997. *ScaLAPACK users’ guide*. SIAM.
- [8] Project Jupyter community. 2022. Project Jupyter Web site. <https://jupyter.org>.
- [9] Ewa Deelman, Rafael Ferreira da Silva, Karan Vahi, Mats Ryngé, Rajiv Mayani, Ryan Tanaka, Wendy R. Whitcup, and Miron Livny. 2021. The Pegasus workflow management system: Translational computer science in practice. *Journal of Computational Science* 52 (2021), 101200.
- [10] Jack J Dongarra. 2022. The evolution of mathematical software. *Commun. ACM* 65, 12 (2022), 66–72.
- [11] J. J. Dongarra, Jeremy Du Croz, Sven Hammarling, and I. S. Duff. 1990. A Set of Level 3 Basic Linear Algebra Subprograms. *ACM Trans. Math.*

- Softw. 16, 1 (March 1990), 1–17. <https://doi.org/10.1145/77626.79170>
- [12] Jack J. Dongarra, Jeremy Du Croz, Sven Hammarling, and Richard J. Hanson. 1988. An Extended Set of FORTRAN Basic Linear Algebra Subprograms. *ACM Trans. Math. Softw.* 14, 1 (March 1988), 1–17. <https://doi.org/10.1145/42288.42291>
- [13] Juan J Durillo and Radu Prodan. 2014. Multi-objective workflow scheduling in Amazon EC2. *Cluster computing* 17, 2 (2014), 169–189.
- [14] Efstratios Gallopoulos, Bernard Philippe, and Ahmed H Sameh. 2016. *Parallelism in matrix computations*. Springer. 3–16 pages.
- [15] Robert Graves, Thomas H Jordan, Scott Callaghan, Ewa Deelman, Edward Field, Gideon Juve, Carl Kesselman, Philip Maechling, Gaurang Mehta, Kevin Milner, et al. 2011. CyberShake: A physics-based seismic hazard model for southern California. *Pure and Applied Geophysics* 168, 3 (2011), 367–381.
- [16] Sachi Gupta, Sailesh Iyer, Gaurav Agarwal, Poongodi Manoharan, Abeer D Algarni, Ghadah Aldehim, and Kaamran Raahemifar. 2022. Efficient prioritization and processor selection schemes for heft algorithm: A makespan optimizer for task scheduling in cloud environment. *Electronics* 11, 16 (2022), 2557.
- [17] Ashraf M Hemeida, SA Hassan, Salem Alkhalaf, MMM Mahmoud, MA Saber, Ayman M Bahaa Eldin, Tomonobu Senjyu, and Abdullah H Alayed. 2020. Optimizing matrix-matrix multiplication on intel’s advanced vector extensions multicore processor. *Ain Shams Engineering Journal* 11, 4 (2020), 1179–1190.
- [18] Raj Jain. 1991. *The art of computer systems performance analysis — techniques for experimental design, measurement, simulation, and modeling*. Wiley. I–XXVII, 1–685 pages.
- [19] Raymes Khoury, Bernd Burgstaller, and Bernhard Scholz. 2011. Accelerating the Execution of Matrix Languages on the Cell Broadband Engine Architecture. *IEEE Transactions on Parallel and Distributed Systems* 22, 1 (2011), 7–21. <https://doi.org/10.1109/TPDS.2010.58>
- [20] Donald E. Knuth. 1997. *The Art of Computer Programming, Volume 2 (3rd Ed.): Seminumerical Algorithms*. Addison-Wesley Longman Publishing Co., Inc., USA.
- [21] Erwin Kreyszig, Herbert Kreyszig, and E. J. Norminton. 2011. *Advanced Engineering Mathematics* (tenth ed.). Wiley, Hoboken, NJ.
- [22] C. L. Lawson, R. J. Hanson, D. R. Kincaid, and F. T. Krogh. 1979. Basic Linear Algebra Subprograms for Fortran Usage. *ACM Trans. Math. Softw.* 5, 3 (Sept. 1979), 308–323. <https://doi.org/10.1145/355841.355847>
- [23] Shigang Li, ChangJun Hu, JunChao Zhang, and Yunquan Zhang. 2015. Automatic tuning of sparse matrix-vector multiplication on multicore clusters. *Science China Information Sciences* 58 (06 2015). <https://doi.org/10.1007/s11432-014-5254-x>
- [24] Jonathan Livny, Hidayat Teonadi, Miron Livny, and Matthew K Waldor. 2008. High-throughput, kingdom-wide prediction and annotation of bacterial non-coding RNAs. *PloS one* 3, 9 (2008), e3197.
- [25] Junior Loff, Renato B. Hoffman, Dalvan Griebler, and Luiz G. Fernandes. 2021. High-Level Stream and Data Parallelism in C++ for Multi-Cores. In *Proceedings of the 25th Brazilian Symposium on Programming Languages (Joinville, Brazil) (SBLP ’21)*. Association for Computing Machinery, New York, NY, USA, 41–48. <https://doi.org/10.1145/3475061.3475078>
- [26] Hadeer Mahmoud, Mostafa Thabet, Mohamed H. Khafagy, and Fatma A. Omara. 2022. Multiobjective Task Scheduling in Cloud Environment Using Decision Tree Algorithm. *IEEE Access* 10 (2022), 36140–36151. <https://doi.org/10.1109/ACCESS.2022.3163273>
- [27] Pierre Michaud. 2012. Demystifying multicore throughput metrics. *IEEE Computer Architecture Letters* 12, 2 (2012), 63–66.
- [28] Yukio Miyasaka, Akihiro Goda, Ashish Mittal, and Masahiro Fujita. 2020. Synthesis and Generalization of Parallel Algorithm for Matrix-vector Multiplication. *IPSS Transactions on System LSI Design Methodology* 13 (01 2020), 31–34. <https://doi.org/10.2197/ipsjtsldm.13.31>
- [29] Thi My Tuyen Nguyen, Yoosang Park, Jaeyoung Choi, and Raehyun Kim. 2020. Evaluating performance of Parallel Matrix Multiplication Routine on Intel KNL and Xeon Scalable Processors. In *2020 IEEE International Conference on Autonomic Computing and Self-Organizing Systems Companion (ACSOS-C)*. 42–47. <https://doi.org/10.1109/ACSOS-C51401.2020.00027>
- [30] Wang Qian, Zhang Xianyi, and Zhang Yunquan. 2022. OpenBLAS: An Optimized BLAS Library. <https://www.openblas.net/>.
- [31] Ravi Reddy, Alexey Lastovetsky, and Pedro Alonso. 2009. HeteroP-BLAS: A set of Parallel Basic Linear Algebra Subprograms optimized for heterogeneous computational clusters. *Scalable Computing: Practice and Experience* 10, 2 (2009).
- [32] Yassir Samadi, Mostapha Zbakh, and Claude Tadonki. 2018. E-HEFT: Enhancement Heterogeneous Earliest Finish Time algorithm for Task Scheduling based on Load Balancing in Cloud Computing. In *2018 International Conference on High Performance Computing Simulation (HPCS)*. 601–609. <https://doi.org/10.1109/HPCS.2018.00100>
- [33] Shigeyuki Sato and Hideya Iwasaki. 2011. Automatic Parallelization via Matrix Multiplication. *ACM SIGPLAN Notices* 46, 470–479. <https://doi.org/10.1145/1993498.1993554>
- [34] Amazon Web Services. 2022. Amazon EC2 C5 Instances. <https://aws.amazon.com/ec2/instance-types/c5>.
- [35] John A. Stratton, Christopher I. Rodrigues, I-Jui Sung, Nady Obeid, Li-Wen Chang, Nasser Anssari, Geng Liu, and Wen mei W. Hwu. 2012. Parboil: A Revised Benchmark Suite for Scientific and Commercial Throughput Computing.
- [36] Ian J Taylor, Ewa Deelman, Dennis B Gannon, et al. 2007. *Workflows for e-Science: scientific workflows for grids*. Vol. 1. Springer.
- [37] H. Topcuoglu, S. Hariri, and Min-You Wu. 2002. Performance-effective and low-complexity task scheduling for heterogeneous computing. *IEEE Transactions on Parallel and Distributed Systems* 13, 3 (2002), 260–274. <https://doi.org/10.1109/71.993206>
- [38] Jeffrey D. Ullman. 1975. NP-complete scheduling problems. *Journal of Computer and System sciences* 10, 3 (1975), 384–393.
- [39] Robert A Van De Geijn and Jerrell Watts. 1997. SUMMA: Scalable universal matrix multiplication algorithm. *Concurrency: Practice and Experience* 9, 4 (1997), 255–274.
- [40] Qian Wang, Xianyi Zhang, Yunquan Zhang, and Qing Yi. 2013. AUGEM: automatically generate high performance dense linear algebra kernels on x86 CPUs. In *SC’13: Proceedings of the International Conference on High Performance Computing, Networking, Storage and Analysis*. IEEE, 1–12.
- [41] Zhang Xianyi, Wang Qian, and Zhang Yunquan. 2012. Model-driven level 3 BLAS performance optimization on Loongson 3A processor. In *2012 IEEE 18th international conference on parallel and distributed systems*. IEEE, 684–691.
- [42] Shinhyung Yang, Jiun Jeong, Bernhard Scholz, and Bernd Burgstaller. 2022. Cloudprofiler: TSC-based inter-node profiling and high-throughput data ingestion for cloud streaming workloads. <https://doi.org/10.48550/ARXIV.2205.09325>
- [43] Honglin Zhang, Yaohua Wu, and Zaixing Sun. 2022. EHEFT-R: multi-objective task scheduling scheme in cloud computing. *Complex and Intelligent Systems* 8 (2022), 4475–4482. <https://doi.org/10.1007/s40747-021-00479-7>
- [44] Xiangchen Zhao, Diyi Hu, and Bhaskar Krishnamachari. 2021. Design and Experimental Evaluation of Algorithms for Optimizing the Throughput of Dispersed Computing. <https://doi.org/10.48550/ARXIV.2112.13875> arXiv:2112.13875